Received: 4 May 2023 | Revised: 24 May 2023 | Accepted: 24 May 2023

DOI: 10.1002/agt2.364

Aggregate WILEY Open Access

RESEARCH ARTICLE

Design of AIEgen-based porphyrin for efficient heterogeneous photocatalytic hydrogen evolution

Special Collection: Aggregation-Induced Processes and Functions

Govardhana Babu Bodedla[1,2,3] | **Muhammad Imran**[4] | **Jianzhang Zhao**[4] | **Xunjin Zhu**[3] | **Wai-Yeung Wong**[1,2]

[1]Department of Applied Biology & Chemical Technology and Research Institute for Smart Energy, The Hong Kong Polytechnic University, Hong Kong, P. R. China

[2]The Hong Kong Polytechnic University Shenzhen Research Institute, Shenzhen, P. R. China

[3]Department of Chemistry, Hong Kong Baptist University, Hong Kong, P. R. China

[4]State Key Laboratory of Fine Chemicals and School of Chemical Engineering, Dalian University of Technology, Dalian, P. R. China

Correspondence
Wai-Yeung Wong, Department of Applied Biology & Chemical Technology and Research Institute for Smart Energy, The Hong Kong Polytechnic University, Hong Kong SAR, P. R. China.
Email: wai-yeung.wong@polyu.edu.hk

Xunjin Zhu, Department of Chemistry, Hong Kong Baptist University, Hong Kong SAR, P. R. China.
Email: xjzhu@hkbu.edu.hk

Funding information
RGC Senior Research Fellowship Scheme, Grant/Award Number: SRFS2021-5S01; National Natural Science Foundation of China, Grant/Award Number: 52073242; Hong Kong Polytechnic University, Grant/Award Number: YXA2; Research Institute for Smart Energy, Grant/Award Number: CDAQ; Miss Clarea Au for the Endowed Professorship in Energy, Grant/Award Number: 847S; General Research Fund, Grant/Award Numbers: HKBU 12304320, N_HKBU213/22; Hong Kong Research Grants Council, and Initiation Grant for Faculty Niche Research Areas (IG-FNRA), Grant/Award Number: 2020/21

Abstract

Tetraphenylethylene (TPE)-conjugated porphyrin TPE-ZnPF is synthesized in high yield and characterized by single-crystal X-ray diffraction. The propeller-shaped TPE groups not only enable exceptional aggregation-induced emission (AIE) in the solid state but also abolish the strong π-π stacking of porphyrin moieties and thus prohibit aggregation-caused quenching (ACQ). TPE-ZnPF aggregates feature long-lived photoexcited states, which subsequently suppress non-radiative decay channels and enhance emission intensity. Moreover, its aggregates show more efficient light-harvesting ability due to the Förster resonance energy transfer from the TPE energy donor to the porphyrin core energy acceptor, well-defined nanosphere morphology, and more efficient photoinduced charge separation than the porphyrin Ph-ZnPF, which possesses ACQ and agglomerated morphology. As a result, an excellent photocatalytic hydrogen evolution rate (ηH_2) of 56.20 mmol g^{-1} h^{-1} is recorded for TPE-ZnPF aggregates, which is 94-fold higher than that of the aggregates of Ph-ZnPF (0.60 mmol g^{-1} h^{-1}) without the TPE groups.

KEYWORDS
aggregation-induced emission, AIEgen, porphyrin, π-π-stacking, photocatalytic hydrogen evolution

1 | INTRODUCTION

Photocatalytic hydrogen evolution (PHE) is a promising sustainable green energy technology that can solve the global warming issues resulting from the combustion of fossil fuels.[1–3] Typically, irradiation of solar light on a photocatalytic system containing a photosensitizer, sacrificial donor, cocatalyst, and water produces hydrogen. In recent times, designing high-performance photosensitizers gained much attention from the scientific society.[1,4–13] In this context, porphyrin-based sensitizers received great interest due to their high light-harvesting ability in the UV-Visible region, multiple redox states for attaining efficient photoinduced charge separation, and high photostability during photocatalysis.[1] Besides, their optoelectronic properties can be easily adjusted by integration of chromophores at four *meso*-positions of porphyrin macrocycle and insertion of various metals inside the porphyrin ring and consequently tailorable PHE properties.[1] However, most porphyrins exhibit aggregation-caused quenching (ACQ) of photoluminescence in the solid state due to the strong π-π stacking of planar porphyrin moieties.[14,15] This tendency activates the non-radiative decay channels which further shorten the electron lifetimes (τ_{PL}) of photoexcited states and subsequently low photoluminescence quantum yields (Φ_{PL}) and therefore inferior PHE performance of porphyrin-based photosensitizers.

On the other hand, aggregation-induced emission (AIE) active propeller-shaped tetraphenylethylene (TPE) chromophore commonly called as AIEgen would abolish the

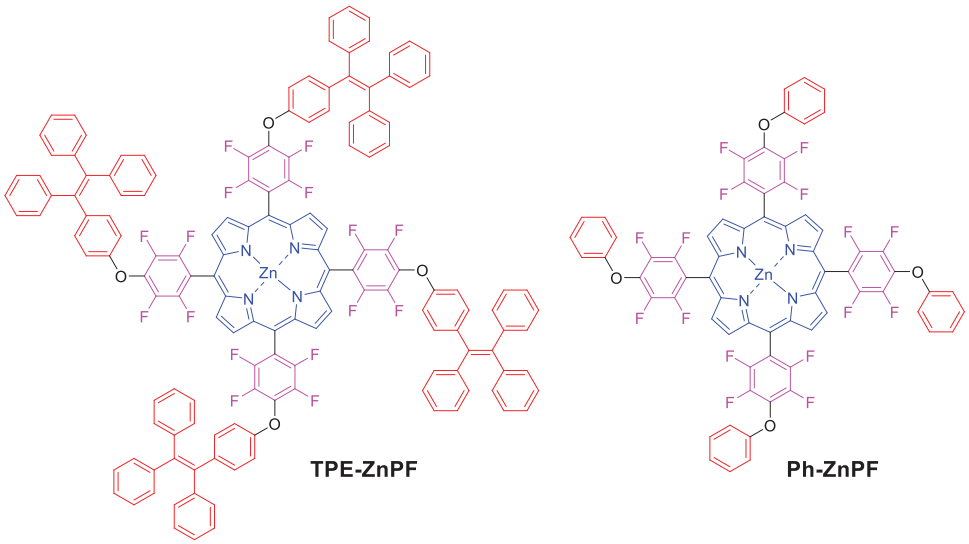

FIGURE 1 Structures of porphyrins used in this study.

strong π-π stacking of planar porphyrin moieties in the aggregated state and thus prohibit ACQ.[16–18] Moreover, TPE enhances the photoluminescence of its derivatives in the solid state by suppressing non-radiative decay channels via restriction of intramolecular motions and consequently leads to improved Φ_{PL}.[19] Hence, conjugation of TPE moieties to the *meso*-positions of the porphyrin ring through a suitable π-linker would suppress ACQ and enhance emission intensity through AIE which subsequently provides longer τ_{PL} of photoexcited states in porphyrins in their aggregated states and hence expectable efficient electron transfer from photoexcited porphyrin aggregates to the proton for water reduction in the PHE process. Additionally, due to the emission range of TPE chromophore lying within 400–450 nm and Soret-band absorption of porphyrin ring falls in the range 400–450 nm, an efficient Förster resonance energy transfer (FRET) from TPE moieties to porphyrin ring can be possible and hence improved light-harvesting nature in the entire UV-Vis region for TPE-conjugated porphyrin can be obtained. More notably, though an iridium motif-conjugated porphyrin with AIE was developed for PHE, this porphyrin did not exhibit AIE completely in the aggregated states.[20] Furthermore, synthesis of such noble-metal-based iridium motif-conjugated porphyrin involves complicated synthetic protocol and is also not much photostable and hence is not economically viable for efficient and long-term PHE technology. Thus, we presumed that an easily synthesizable and cost-effective TPE-conjugated porphyrin is an ideal approach to advance the PHE technology. Keeping all these points in mind, we have developed a TPE-conjugated porphyrin TPE-ZnPF (Figure 1) through an easy synthetic protocol (Scheme 1) to study the effect of AIE on the PHE of TPE-ZnPF porphyrin aggregates. Controlled ACQ porphyrin Ph-ZnPF with phenylene moieties was also synthesized for comparison purposes.

2 | RESULTS AND DISCUSSION

The synthesis of TPE-ZnPF and Ph-ZnPF is shown in Scheme 1. Both TPE-ZnPF and Ph-ZnPF were unambiguously characterized by nuclear magnetic resonance and matrix-assisted laser desorption ionization–time-of-flight. Especially, TPE-ZnPF was confirmed by single-crystal X-ray diffraction (CCDC 2219954) (Figure 2). Free-base porphyrin (TPE-PFNH2) of TPE-ZnPF was also confirmed by single-crystal X-ray diffraction (CCDC 2219955) (Figure S3). The top and side views of single-crystal structures, the dihedral angles between moieties in single-crystal structures, and the packing diagram in the unit cell of single-crystals are shown in Figures S1–S8.

2.1 | Optoelectronic and morphological studies

The absorption and emission spectra of porphyrins and TPE-OH are shown in Figure 3 and the corresponding data are noted in Table 1. As seen in Figure 3A, both porphyrins showed typical Soret-band (ca. 420 nm) and Q-band (ca. 500–650 nm) absorption peaks of porphyrin moiety in tetrahydrofuran (THF) solution. In addition, the peak at 320 nm belongs to the TPE moiety in TPE-ZnPF. This is witnessed as the appearance of absorption peaks at 320 nm for TPE-OH. Noteworthily, the absorption profile of TPE-ZnPF is highly red-shifted and broadened in THF/water (H_2O) mixture solution compared to that in THF solution, implying the formation of *J*-type aggregates in THF/H_2O.[15] In the case of Ph-ZnPF, the absorption profile is slightly red-shifted and broadened in THF/H_2O in comparison to that in THF. Obviously, TPE-ZnPF aggregates cover a much broader absorption spectrum from 290 to 920 nm than Ph-ZnPF aggregates. It indicates that the conjugation of UV light-absorbing TPE chromophores to the porphyrin core is a facile molecular design to effectively improve the light-harvesting property of porphyrins in the UV-Vis region. This result further signifies that the TPE-ZnPF can be employed as a potential photosensitizer for heterogeneous PHE (vide infra). The morphology of such aggregates was further studied by scanning electron microscopy (SEM) (Figure 4A,B and Figures S11 and S12). The aggregates of TPE-ZnPF possessed well-defined nanosphere morphology (150–250 nm), while agglomerates were observed for Ph-ZnPF. The

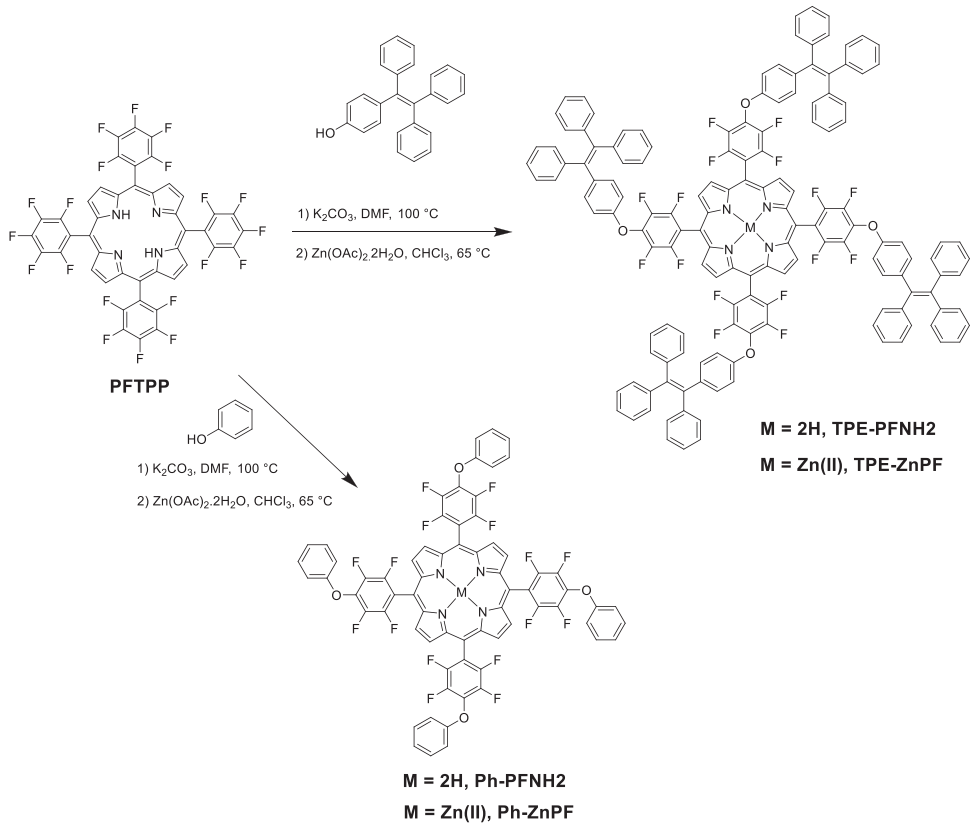

SCHEME 1 Synthetic scheme of TPE-ZnPF and Ph-ZnPF.

TABLE 1 Photophysical and electrochemical properties of TPE-ZnPF, Ph-ZnPF, and TPE-OH.

Compound	λ_{abs}[a] ($\varepsilon \times 10^4$, M^{-1} cm^{-1}) (nm)	λ_{abs}[b] ($\varepsilon \times 10^4$, M^{-1} cm^{-1}) (nm)	λ_{em}[a] (nm)	λ_{em}[b] (nm)	τ_{PL}[a] (ns)	τ_{PL}[b] (ns)	Φ_{PL}[a,c]	Φ_{PL}[b,c]	E_{Ox}[d] (eV)	E_{Red}[e] (eV)	$E_{(P^+/P^*)}$[f] (eV)	$E(P^*/P^-)$[g] (eV)	$E_{0\text{-}0}$[h] (eV)
TPE-ZnPF	242 (11.4), 320 (7.6), 422 (23.2), 552 (2.6), 589 (0.4)	334 (10.0), 447 (14.1), 560 (7.7), 591 (5.9)	595, 647	597, 647	1.70	3.60	0.12	0.30	1.16, 1.49, 1.69	−0.78	−1.03	1.41	2.19
Ph-ZnPF	419 (19.5), 549 (0.9), 586 (0.1)	425 (10.1), 552 (2.2), 587 (1.2)	591, 645	592, 646	1.80	0.80	0.12	0.06	1.18, 1.60, 1.84	−0.78	−1.04	1.44	2.22
TPE-OH	248 (2.6), 319 (1.2)		389	391	–	–	–	–					

[a]THF solution (10 μM).
[b]f_w of 95% in THF/H_2O mixture (10 μM).
[c]5,10,15,20-tetraphenylporphyrin (TPP) in degassed toluene was used as a reference (λ_{exc} = 552 nm) with Φ_{PL} = 0.12.
[d]E_{ox} (vs NHE) = 0.77 + E_{ox} (vs Ferrocene).
[e]E_{red} (vs NHE) = 0.77 – E_{red} (vs Ferrocene).
[f]$E_{(P^+/P^*)}$ (vs NHE) = E_{Ox} – $E_{0\text{-}0}$; here "P" refers to porphyrin photosensitizer.
[g]$E_{(P^*/P^-)}$ (vs NHE) = E_{Red} + $E_{0\text{-}0}$.
[h]Estimated from the intersection of the normalized absorption and emission spectra.

nano-sized aggregates of TPE-ZnPF are useful to provide a large active surface area and thereby more photocatalytic reactive sites on the surface of TPE-ZnPF and simultaneously enhanced PHE than agglomerated morphology of Ph-ZnPF.[21] Moreover, dynamic light scattering analysis (Figure S13) indicates that the average size of TPE-ZnPF aggregates is 189.0 nm which also matches the SEM analysis. As seen in Figure 3B, both porphyrins exhibited two emission peaks in the range of 600–700 nm under the excitation of Soret-band absorption (420 nm), revealing that they are related to the porphyrin ring. Importantly, when the emission spectrum of TPE-ZnPF was recorded under the excitation of TPE absorption (320 nm), the emission peak at around 370 nm which corresponds to TPE chromophore disappeared, and the intensity of porphyrin emission peaks was enhanced by 2-fold. This could be attributed to the complete FRET from the TPE energy donor to the porphyrin energy acceptor. Since the emission spectrum of TPE-OH and the absorption spectrum of Ph-ZnPF overlapped extremely well, there is an expected FRET from TPE groups to the porphyrin ring in

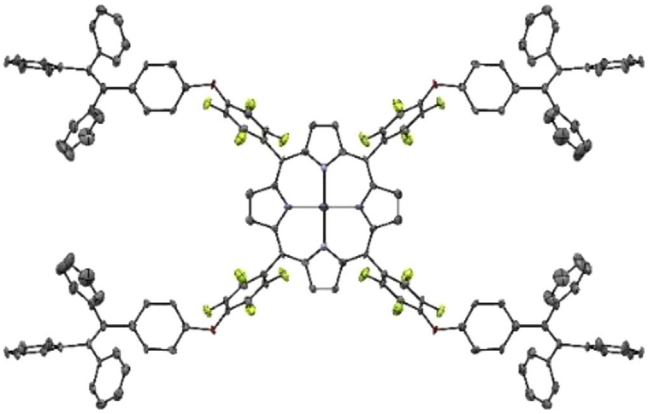

FIGURE 2 Single-crystal structure of TPE-ZnPF (hydrogen atoms are omitted for clarity).

TPE-ZnPF (Figure S18A).[22] The FRET occurrence is also much beneficial to enhance the light-harvesting ability and thereby stabilize the photoexcited states of TPE-ZnPF.[18,20]

The AIE properties of TPE-ZnPF were examined in THF/H_2O solvent mixture. As shown in Figure 3C, the emission intensity of TPE-ZnPF is gradually enhanced with increasing water fraction (f_w) from 0% to 95% in THF/H_2O mixture. It indicates that integration of propeller-shaped TPE groups to the porphyrin ring would efficiently reduce the strong π-π stacking of TPE-ZnPF in the solid state and thus prohibit ACQ, which subsequently suppresses the non-radiative decay channels and induces the AIE property for TPE-ZnPF. The AIE property could further stabilize the photoexcited states of TPE-ZnPF and consequently lead to longer τ_{PL} in the aggregated state. This was further confirmed by measuring τ_{PL} of TPE-ZnPF in THF/H_2O mixture and THF solvent. It was found that the calculated τ_{PL} of TPE-ZnPF in f_w = 95% of THF/H_2O solvent mixture is 3.6 ns which is 2-fold higher than τ_{PL} (1.7 ns) recorded in THF solvent. On the other hand, the calculated Φ_{PL} of TPE-ZnPF in f_w = 95% of THF/H_2O mixture is also higher than that in THF solvent (Table 1). This result is also consistent with the τ_{PL} values. Similarly, the free-base porphyrin TPE-PFNH2 of TPE-ZnPF also showed the AIE property in THF/H_2O solvent mixture (Figure S19B). On the contrary, the control porphyrin Ph-ZnPF possessing only phenolic moieties showed decreased emission intensity when increasing f_w in THF/H_2O mixture (Figure 3D), which indicates that Ph-ZnPF severely suffers from ACQ. The τ_{PL} and Φ_{PL} values of Ph-ZnPF also depict the strong ACQ (Table 1). On the other hand, the TPE derivative TPE-OH has shown excellent AIE in THF/H_2O mixture (Figure S19A). All these results clearly demonstrated that the integration of TPE moieties to the porphyrin core in TPE-ZnPF can provide long-lived photoexcited states by reducing the non-radiative decay channels and thus higher PHE performance compared to Ph-ZnPF (vide infra).

The excited-state oxidation ($E_{(P^+/P^*)}$) and reduction ($E_{(P^*/P^-)}$) potential values of TPE-ZnPF and Ph-ZnPF were estimated by performing cyclic voltammetric experiments (Figure S20A).[23,24] The data is shown in Table 1. As shown in Figure S20B, the energy levels of $E_{(P^+/P^*)}$ of both porphyrins are high-lying than H_2/H^+ reduction potential and the energy levels of $E_{(P^*/P^-)}$ are low-lying than TEA redox potential. It suggests that electron transfer from photoexcited states of porphyrins to proton and regeneration of oxidized porphyrins by TEA are thermodynamically favorable during the PHE cycle.

2.2 | Theoretical calculations

Theoretical calculations were carried out for the rationalization of the photophysical properties of the porphyrins. The optimized ground state geometries of TPE-ZnPF and Ph-ZnPF are shown in Figure 5A,B. For both cases, the dihedral angles between fluorinated aryl rings and porphyrin core are almost the same (71.7°–73.6°), which is typical for *meso*-tetra(phenyl)porphyrin. However, in TPE-ZnPF the dihedral angles between TPE units and fluorinated phenyl rings are in the range of 62.7°–65.5°, which are smaller than the dihedral angles between the adjacent phenyl moiety and fluorinated phenyl rings in Ph-ZnPF (82.1°). This smaller dihedral angle in TPE-ZnPF may induce larger electronic coupling between the two units. This result is in accordance with the efficient FRET from TPE units to porphyrin moiety (vide supra). Moreover, the highest occupied molecular orbital (HOMO) of TPE-ZnPF is completely confined to the porphyrin moiety, and the lowest unoccupied molecular orbital (LUMO) is localized on the TPE unit; therefore, the transition of HOMO to LUMO consists of charge transfer feature from TPE units to porphyrin center (Figure S10). On the contrary, both HOMO and LUMO are localized on the porphyrin ring in Ph-ZnPF indicating a lack of charge transfer ability (Figure S10). The TPE-ZnPF showed a higher dipole moment value of 1.08 D than Ph-ZnPF with 0.67 D. Since TPE-ZnPF possesses charge transfer character and high dipole moment value, it is expected to have a more efficient photoinduced charge separation than Ph-ZnPF and hence higher PHE for the former (vide infra).[25]

2.3 | PHE studies

PHE was evaluated in a photocatalytic system consisting of porphyrin photosensitizer (PS), TEA sacrificial donor, Pt cocatalyst, and THF/H_2O proton source. Typically, we used a THF/H_2O (0.5:9.5, v/v) mixture to maintain the highest degree of AIE property and correlate the obtained PHE data with photophysical properties. As shown in Figure 6A, TPE-ZnPF produced a PHE rate (ηH_2) of 56.20 mmol g^{-1} h^{-1}. Under the same conditions, Ph-ZnPF delivered a ηH_2 of 0.60 mmol g^{-1} h^{-1} which is much lower than that of TPE-ZnPF. This result undoubtedly indicates that the AIE phenomenon played an important role to enhance the PHE of TPE-ZnPF. The effect of the degree of AIE on the PHE performance of TPE-ZnPF was studied as well. The ηH_2 of the TPE-ZnPF photocatalytic system increased with increasing f_w in THF/H_2O mixture (Figure 6B). This result clearly demonstrates that TPE groups reduced the strong π-π interactions between planar porphyrin moieties in the aggregated state of TPE-ZnPF which resulted in suppressed non-radiative decay channels and thus enhanced photoluminescence and thereby long-lived photoexcited states. Subsequently, this leads to an efficient electron transfer from long-lived photoexcited states of TPE-ZnPF to Pt cocatalyst for proton reduction. Moreover, the ηH_2 of the photocatalytic system of TPE-ZnPF is the highest value among

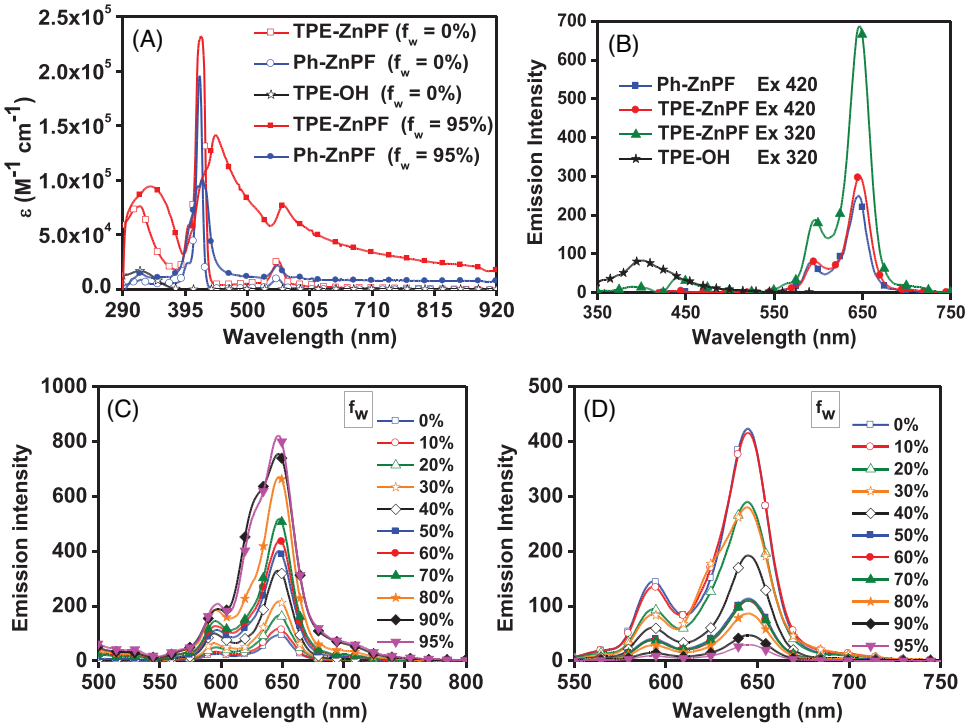

FIGURE 3 Absorption (A) and emission (B) spectra of Ph-ZnPF, TPE-ZnPF, and TPE-OH recorded in tetrahydrofuran (THF) (10 μM), the emission spectrum of (C) TPE-ZnPF and (D) Ph-ZnPF recorded in different ratio of f_w from 0% to 95% in THF/H_2O mixture.

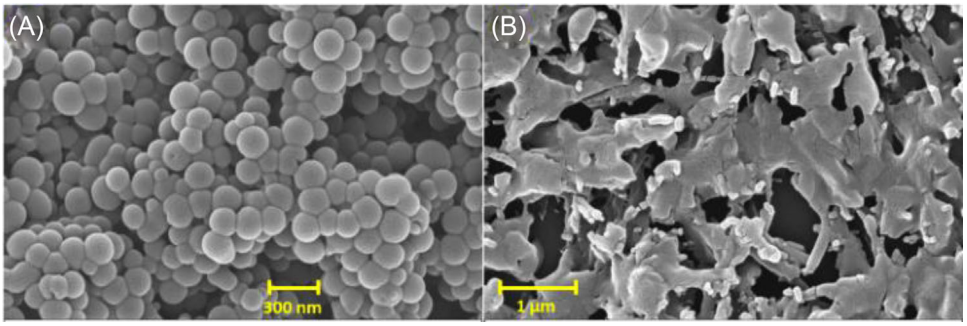

FIGURE 4 Typical SEM images of (A) TPE-ZnPF and (B) Ph-ZnPF aggregates in THF/H_2O (0.5:9.5, v/v).

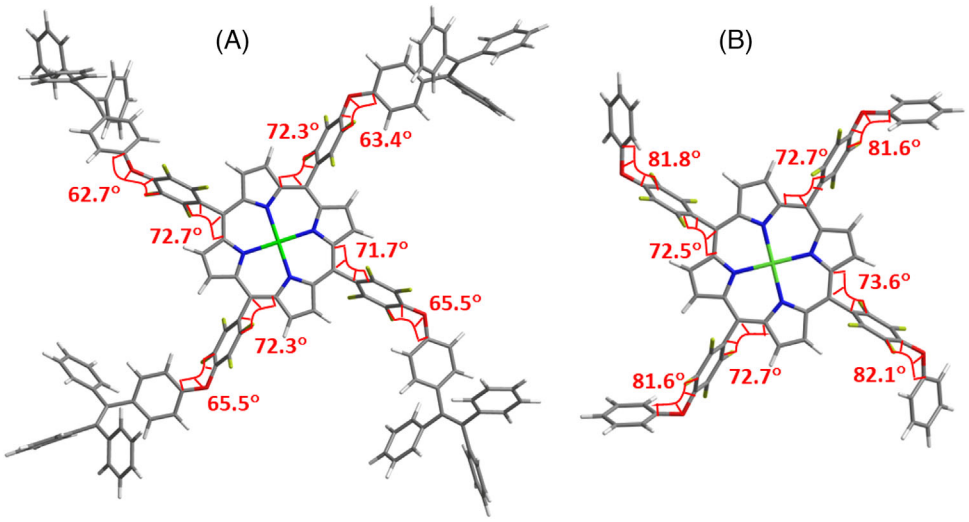

FIGURE 5 Optimized geometries of (A) TPE-ZnPF and (B) Ph-ZnPF.

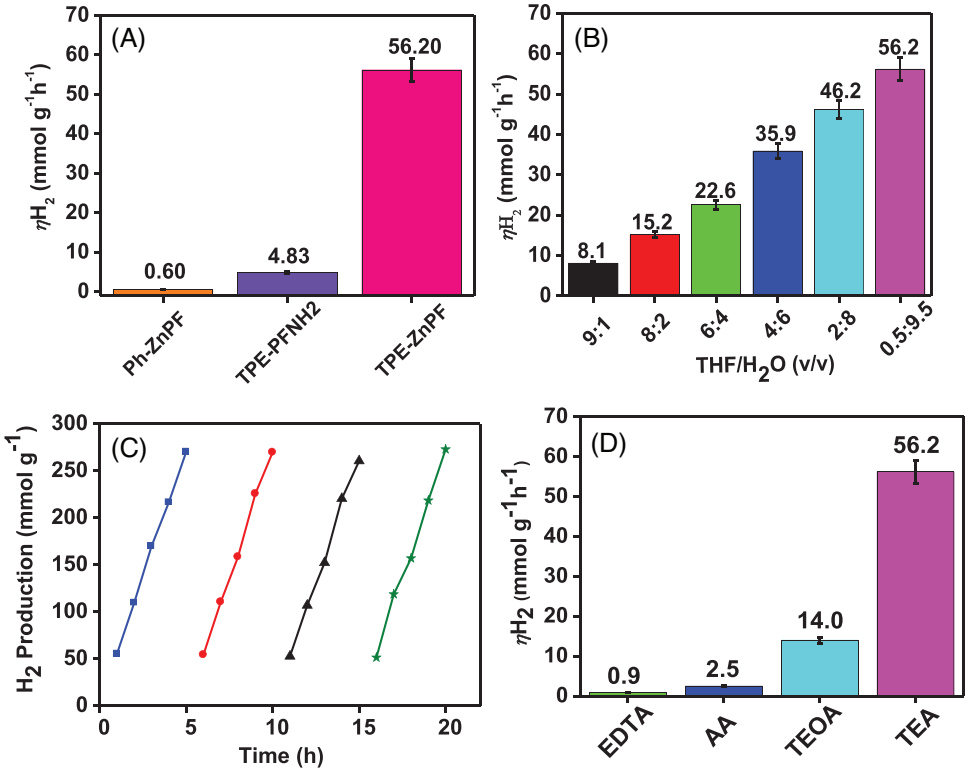

FIGURE 6 (A) ηH_2 of photocatalytic systems of Ph-ZnPF, TPE-PFNH2, and TPE-ZnPF under irradiation for 5 h: PS (10 μM) + TEA (0.3 M) + THF/H_2O (0.5:9.5 v/v) + Pt (3 wt%), (B) ηH_2 of photocatalytic systems of TPE-ZnPF under irradiation for 5 h: PS (10 μM) + TEA (0.3 M) + THF/H_2O + Pt (3 wt%), (C) H_2 production of different cycles of TPE-ZnPF photocatalytic system: TEA was re-added after third cycle and (D) ηH_2 of photocatalytic systems of TPE-ZnPF under irradiation for 5 h: PS (10 μM) + EDTA (ethylenediaminetetraacetic acid)/AA (ascorbic acid)/TEOA (triethanolamine)/TEA (0.3 M) + THF/H_2O (0.5:9.5 v/v) + Pt (3 wt%) (white LED light (148.5 mW cm^{-2})).

noble-metal-free porphyrin small molecules reported so far.[1,26,27] The photostability of TPE-ZnPF was verified by calculating ηH_2 for four consecutive PHE experiments of the photocatalytic system under 20 h light irradiation (Figure 6C). From Figure 6C, the ηH_2 of the photocatalytic system does not show any obvious degradation in each cycle. The nanosphere morphology of TPE-ZnPF also did not change before and after 20 h light irradiation (Figure S14). It implies that TPE-ZnPF holds good photostability. To further improve the PHE of TPE-ZnPF, we also varied the different sacrificial donors (Figure 6D) and the concentration of TEA (Figure S21), and the amount of Pt in the photocatalytic systems (Figure S22). Obviously, these results imply that the PHE data shown in Figure 6A corresponds to the most optimized PHE for TPE-ZnPF. Moreover, under the optimized PHE conditions of TPE-ZnPF, free-base porphyrin TPE-PFNH2 showed a lower ηH_2 than that of TPE-ZnPF. It indicates that Zn metal is very important for enhanced PHE. However, the ηH_2 of TPE-PFNH2 is 8-fold higher than Ph-ZnPF, indicating the importance of TPE conjugation to the porphyrin macrocycle. Nevertheless, the photocatalytic system of TPE-ZnPF in the presence of the chloro(pyridine)cobaloxime (CoPyCl) cocatalyst exhibited ηH_2 of 9.12 mmol g^{-1} h^{-1} which is 6-fold lower than that of the Pt cocatalyst-based photocatalytic system (Figure S23).

The photoinduced charge separation and migration of charged carriers of photosensitizers also dictate the performance of the PHE system.[28] As the response in the photocurrent-time (i-t curves) relates to the photoinduced charged species separation of photosensitizer, the porphyrin aggregates coated on indium tin oxide (ITO) were prepared. As shown in Figure 7A, the TPE-ZnPF aggregates showed higher current density in the i-t curves than that of Ph-ZnPF aggregates indicating more efficient photoinduced charge separation and migration of charged species such as holes and electrons for the former porphyrin aggregates. This result is in accordance with the higher PHE of the photocatalytic system of TPE-ZnPF porphyrin aggregates than the Ph-ZnPF porphyrin aggregates photocatalytic system. A feasible PHE mechanism of the photocatalytic systems of porphyrins is shown in Figure 7B. Under light illumination, the ground state porphyrins undergo photoexcitation which results in photoexcited porphyrins and these highly reactive photoexcited porphyrins are further reduced by gaining electrons from the TEA. Subsequently, the reduced porphyrins transfer electrons to the Pt nanoparticles where protons are converted to hydrogen and the porphyrins finally return to the ground state.

3 | CONCLUSIONS

A simple molecular design tactic was explored to convert porphyrins from ACQ to AIE in the solid state by integrating AIEgen TPE moieties into the porphyrin core. The developed TPE-ZnPF significantly showed FRET between TPE and porphyrin ring and thereby improved light-harvesting ability. The AIE property further prompted long-lived photoexcited states of TPE-ZnPF in the solid state and thus longer τ_{PL} value than Ph-ZnPF with ACQ phenomenon. Photocurrent-time correlation and DFT studies indicated that TPE-ZnPF

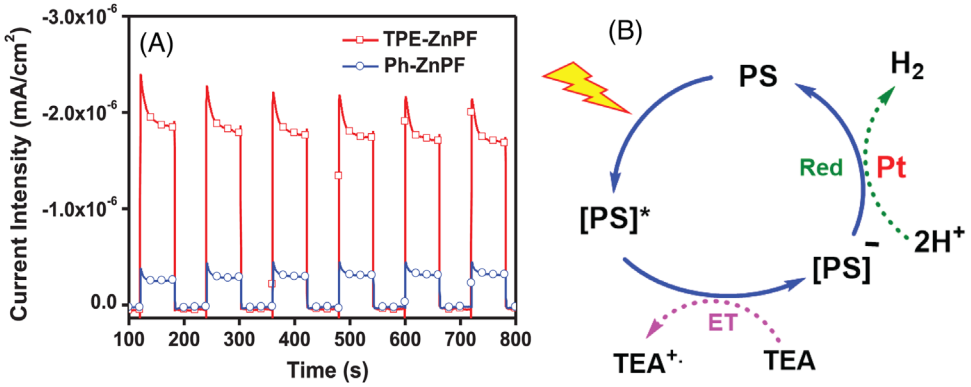

FIGURE 7 (A) I-t response spectra of porphyrins recorded on ITO substrate and (B) feasible PHE mechanism of photocatalytic systems: PS is a photosensitizer, ET refers to electron transfer, and Red represents reduction.

possesses much more efficient photoinduced charge separation than Ph-ZnPF. TPE-ZnPF aggregates also possess well-defined nanosphere morphology while agglomerated morphology was assigned to Ph-ZnPF which indicates more photocatalytic reactive sites for TPE-ZnPF aggregates. As a consequence of high light-harvesting ability, long-lived photoexcited states, and elevated photoinduced charge separation, TPE-ZnPF aggregates produced a very high ηH_2 of 56.20 mmol g^{-1} h^{-1}, which is 94-fold higher than that of Ph-ZnPF (0.60 mmol g^{-1} h^{-1}).

ACKNOWLEDGMENTS

W.-Y. W. acknowledges the financial support from the RGC Senior Research Fellowship Scheme (SRFS2021-5S01), the National Natural Science Foundation of China (52073242), the Hong Kong Polytechnic University (YXA2), Research Institute for Smart Energy (CDAQ) and Miss Clarea Au for the Endowed Professorship in Energy (847S). The research was also supported by the General Research Fund (HKBU 12304320 and N_HKBU213/22) from the Hong Kong Research Grants Council, and Initiation Grant for Faculty Niche Research Areas (IG-FNRA) (2020/21)-RC-FNRA-IG/20-21/SCI/06 from Research Committee of Hong Kong Baptist University. We are also thankful to Dr. Leon Li-Min Zhang from The Hong Kong Polytechnic University for helping in the single-crystal XRD analysis of the porphyrins.

CONFLICT OF INTEREST STATEMENT

The authors declare no conflict of interest.

ORCID

Govardhana Babu Bodedla https://orcid.org/0000-0002-8561-2713
Muhammad Imran https://orcid.org/0000-0002-9796-4142
Wai-Yeung Wong https://orcid.org/0000-0002-9949-7525

REFERENCES

1. J. S. O'Neill, L. Kearney, M. P. Brandon, M. T. Pryce, *Coord. Chem. Rev.* **2022**, *467*, 214599.
2. W. Zhang, W. Lai, R. Cao, *Chem. Rev.* **2017**, *117*, 3717.
3. X. Zhang, T. Peng, S. Song, *J. Mater. Chem. A* **2016**, *4*, 2365.
4. D. N. Tritton, F.-K. Tang, G. B. Bodedla, F.-W. Lee, C.-S. Kwan, K. C.-F. Leung, X. Zhu, W.-Y. Wong, *Coord. Chem. Rev.* **2022**, *459*, 214390.
5. S. Liu, P. Lin, M. Wu, Z.-A. Lan, H. Zhuzhang, M. Han, Y. Fan, X. Chen, X. Wang, Q. Li, Z. Li, *Appl. Catal. B: Environ.* **2022**, *309*, 121257.
6. P. Buday, C. Kasahara, E. Hofmeister, D. Kowalczyk, M. K. Farh, S. Riediger, M. Schulz, M. Wächtler, S. Furukawa, M. Saito, D. Ziegenbalg, S. Gräfe, P. Bäuerle, S. Kupfer, B. Dietzek-Ivanšić, W. Weigand, *Angew. Chem. Int. Ed.* **2022**, *61*, e202202079.
7. Y. Liu, J. Wu, F. Wang, *Appl. Catal. B: Environ.* **2022**, *307*, 121144.
8. G. B. Bodedla, Y. Dong, G. Tang, J. Zhao, F. Zhang, X. Zhu, W.-Y. Wong, *J. Mater. Chem. A* **2022**, *10*, 13402.
9. A. C. Yüzer, E. Genc, G. Kurtay, G. Yanalak, E. Aslan, E. Harputlu, K. Ocakoglu, I. Hatay Patir, M. Ince, *Chem. Commun.* **2021**, *57*, 9196.
10. J. Kosco, S. Gonzalez-Carrero, C. T. Howells, T. Fei, Y. Dong, R. Sougrat, G. T. Harrison, Y. Firdaus, R. Sheelamanthula, B. Purushothaman, F. Moruzzi, W. Xu, L. Zhao, A. Basu, S. De Wolf, T. D. Anthopoulos, J. R. Durrant, I. McCulloch, *Nat. Energy* **2022**, *7*, 340.
11. C. Zhang, C. Xie, Y. Gao, X. Tao, C. Ding, F. Fan, H.-L. Jiang, *Angew. Chem. Int. Ed.* **2022**, *61*, e202204108.
12. J. Yang, A. Acharjya, M.-Y. Ye, J. Rabeah, S. Li, Z. Kochovski, S. Youk, J. Roeser, J. Grüneberg, C. Penschke, M. Schwarze, T. Wang, Y. Lu, R. van de Krol, M. Oschatz, R. Schomäcker, P. Saalfrank, A. Thomas, *Angew. Chem. Int. Ed.* **2021**, *60*, 19797.
13. Y. Wang, L. Liu, T. Ma, Y. Zhang, H. Huang, *Adv. Funct. Mater.* **2021**, *31*, 2102540.
14. A. Rananaware, R. S. Bhosale, K. Ohkubo, H. Patil, L. A. Jones, S. L. Jackson, S. Fukuzumi, S. V. Bhosale, S. V. Bhosale, *J. Org. Chem.* **2015**, *80*, 3832.
15. G. B. Bodedla, X. Zhu, W.-Y. Wong, *Aggregate* **2023**, e330. https://doi.org/10.1002/agt2.330
16. Y. Zhang, Y. Zhao, Z. Han, R. Zhang, P. Du, Y. Wu, X. Lu, *Angew. Chem. Int. Ed.* **2020**, *59*, 23261.
17. B. Guo, X. Cai, S. Xu, S. M. A. Fateminia, J. Liu, J. Liang, G. Feng, W. Wu, B. Liu, *J. Mater. Chem. B* **2016**, *4*, 4690.
18. Q. Wang, Q. Chen, G. Jiang, M. Xia, M. Wang, Y. Li, X. Ma, J. Wang, X. Gu, *Chin. Chem. Lett.* **2019**, *30*, 1965.
19. J. Mei, N. L. C. Leung, R. T. K. Kwok, J. W. Y. Lam, B. Z. Tang, *Chem. Rev.* **2015**, *115*, 11718–11940
20. K. Zheng, G. B. Bodedla, Y. Hou, J. Zhang, R. Liang, J. Zhao, D. Lee Phillips, X. Zhu, *J. Mater. Chem. A* **2022**, *10*, 4440.
21. G. B. Bodedla, V. Piradi, M. Imran, J. Zhao, X. Zhu, W.-Y. Wong, *J. Mater. Chem. A* **2023**, *11*, 1473.
22. X. He, L.-H. Xiong, Y. Huang, Z. Zhao, Z. Wang, J. W. Y. Lam, R. T. K. Kwok, B. Z. Tang, *Trends Anal. Chem.* **2020**, *122*, 115743.
23. G. B. Bodedla, W.-Y. Wong, X. Zhu, *J. Mater. Chem. A* **2021**, *9*, 20645.
24. G. B. Bodedla, D. N. Tritton, X. Chen, J. Zhao, Z. Guo, K. C.-F. Leung, W.-Y. Wong, X. Zhu, *ACS Appl. Energy Mater.* **2021**, *4*, 3945.
25. H. Lin, J. Wang, J. Zhao, Y. Zhuang, B. Liu, Y. Zhu, H. Jia, K. Wu, J. Shen, X. Fu, X. Zhang, J. Long, *Angew. Chem. Int. Ed.* **2022**, *134*, e202117645.
26. E. Nikoloudakis, I. López-Duarte, G. Charalambidis, K. Ladomenou, M. Ince, A. G. Coutsolelos, *Chem. Soc. Rev.* **2022**, *51*, 6965
27. M. Joseph, S. Haridas, *Int. J. Hydrog. Energy* **2020**, *45*, 11954.

28. G. B. Bodedla, J. Huang, W.-Y. Wong, X. Zhu, *ACS Appl. Nano Mater.* **2020**, *3*, 7040.

SUPPORTING INFORMATION

Additional supporting information can be found online in the Supporting Information section at the end of this article.

How to cite this article: G. B. Bodedla, M. Imran, J. Zhao, X. Zhu, W. Y. Wong, *Aggregate* **2023**, *4,* e364. https://doi.org/10.1002/agt2.364